

# An Updated Line List for Spectroscopic Investigation of G Stars- I: Redetermination of the Abundances in the Solar Photosphere

T. Şahin<sup>1\*</sup> , M. Marişmak<sup>1</sup> , N. Çınar<sup>1</sup> , and S. Bilir<sup>2</sup> 

<sup>1</sup> Akdeniz University, Faculty of Science, Department of Space Sciences and Technologies 07058, Antalya, Turkey

<sup>2</sup> İstanbul University, Faculty of Science, Department of Astronomy and Space Sciences 34119, Beyazıt, İstanbul, Turkey

## ABSTRACT

We propose a line list that may be useful for the abundance analysis of G-type stars in the wavelength range 4080 – 6780 Å. It is expected that the line list will be useful for surveys/libraries with overlapping spectral regions (e.g. ELODIE/SOPHIE libraries, UVES-580 setting of *Gaia*-ESO), and in particular for the analysis of F- and G-type stars in general. The atomic data are supplemented by detailed references to the sources. We estimated the Solar abundances using stellar lines and the high-resolution Kitt Peak National Observatory (KPNO) spectra of the Sun to determine the uncertainty in the  $\log g f$  values. By undertaking a systematic search that makes use of the lower excitation potential and  $g f$ -values and using revised multiplet table as an initial guide, we identified 363 lines of 24 species that have accurate  $g f$ -values and are free of blends in the spectra of the Sun and a Solar analogue star, HD 218209 (G6V), for which accurate and up-to-date abundances were obtained from both ELODIE and POLARBASE spectra of the star. For the common lines with the *Gaia*-ESO line list v.6 provided by the *Gaia*-ESO collaboration, we discovered significant inconsistencies in the  $g f$ -values for certain lines of varying species.

**Keywords:** Line: identification - Sun: abundances – Sun: fundamental parameters - Stars: individual (HD 218209)

## 1. INTRODUCTION

Mid-spectral type main-sequence stars (F and G-type stars) play a significant role in understanding the Galactic chemical evolution and history of Galactic structure. These stars formed in the early Milky Way or are currently forming, have main-sequence lifetimes comparable to the age of the Galaxy. F and G-type main-sequence stars have an internal structure consisting of a radiative core surrounded by a large envelope. Such structural configuration prevents heavy elements produced in the core from mixing into the stellar atmosphere. Consequently, mid-spectral type stars carry the chemical composition of the molecular cloud in which they were born. The study of the abundances of heavy elements detected in the atmospheres of F and G-type stars provides valuable insights into the Galactic chemical evolution and the history of Galactic structure, as noted by (Pagel & Patchett 1975).

Moreover, these stars offer crucial information about the formation of different populations within the Galaxy, including the halo, thick disc, and thin disc. By analyzing the kinematics and orbital dynamics of stars that have been spectroscopically studied, one can distinguish between these different population groups in the Milky Way. In addition to providing insights into Galactic chemical evolution and the formation of the Galaxy, considering the case for pure spectroscopic analysis, for instance, the  $\alpha$ -element abundances determined through spectroscopic analysis of stars play a crucial role in testing the population membership of host galaxies.

The abundance of elements in a stellar spectrum, such as metallicity ([Fe/H]), can also be used to estimate

the age of the star. This is because the youngest stars have comparatively higher metal abundances and metallicity, while the oldest stars have lower ones ([Placco et al. 2021](#)). Therefore, pure spectroscopic analysis alone provides crucial information about the nature of host galaxies, in addition to insights into the age and chemical composition of individual stars.

The kinematics, orbital dynamics, and chemical properties of stars are not only key in understanding the chemical structure of our Galaxy and its accompanying formation scenarios but also in determining the origins of (metal-poor) young and old G-spectral type stars. In this context, the author's group is currently conducting a comprehensive study involving over 90 metal-poor G-type stars in the Solar neighbourhood. This study aims to investigate the origins of these stars by analyzing their kinematics, orbital dynamics, and chemical properties. This research will shed light on the formation processes and evolutionary pathways of metal-poor G spectral-type stars in our Galaxy.

Furthermore, the author's group has previously conducted a thorough investigation of six metal-poor F-type dwarf stars in the Solar neighbourhood, with  $[Fe/H]$  values ranging from  $-2.4$  to  $-1$  dex. It is worth noting that the studied metal-poor F-type dwarf stars exhibited significant changes in model atmosphere parameters (effective temperature,  $T_{eff}$ ; surface gravity,  $\log g$ ; metallicity,  $[Fe/H]$ ; microturbulence,  $\xi$ ), as reported in the literature. This research, as published in [Şahin & Bilir \(2020\)](#), employed state-of-the-art analysis methods, including classical spectroscopy with the help of ELODIE spectra. By combining these analysis techniques, the authors were able to determine the Galactic origin of these F-type dwarf stars in the Solar neighbourhood.

The determination of accurate metal abundances depends on the accurate determination of model parameters. Current spectroscopic sky survey programs for metal-poor late spectral stars, for example, indicate the need to determine precisely calibrated model parameters for them. These current sky survey programs include *Gaia*-ESO Public Spectroscopic Survey (GES; [Gilmore et al. 2012](#)), GALactic Archaeology with HERMES (GALAH; [Heijmans et al. 2012](#); [De Silva et al. 2015](#); [Martell et al. 2017](#)), the Large Sky Area Multi-Object Fiber Spectroscopic Telescope (LAMOST; [Zhao et al. 2012](#)), the Sloan Extension for Galactic Understanding and Exploration (SEGUE; [Yanny et al. 2009](#)), the Apache Point Observatory Galactic Evolution Experiment (APOGEE; [Allende Prieto et al. 2008](#)), and the RAdial Velocity Experiment (RAVE; [Steinmetz et al. 2006](#)), and demonstrate that precisely determined and calibrated model atmosphere parameters are required in different regions of the electromagnetic spectrum due to differences in adopted observational methods and techniques in these surveys, for which reliable line lists and atomic data are required.

In this study, we present an up-to-date line list for planned spectral analyses in the framework of the comprehensive study mentioned above. HD 218209 of G6V, the most metal-rich star among 90 G type program stars ( $-2.5 < [Fe/H](dex) < -0.5$ ), was selected for the preparation of the line list which is expected to be useful for the surveys/libraries with overlapping spectral regions (e.g. ELODIE library; [Soubiran et al. 2003](#)) and for the analysis of F and G-type stars in general.

This paper is organized as follows. Section 2 provides information concerning the observations. Section 3 explains the procedures used to measure and identify lines, as well as the techniques employed to determine the model parameters and conduct chemical abundance analyses of both HD 218209 and the Sun. Section 4 is dedicated to discussing findings and their potential implications.

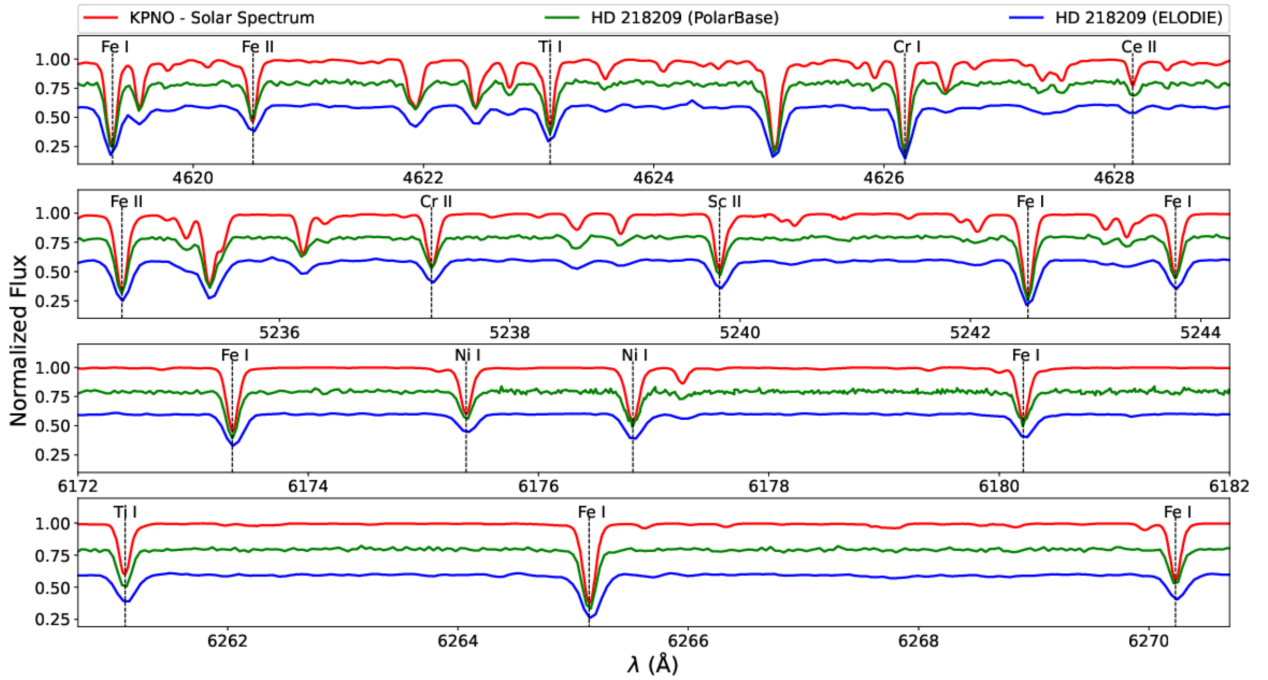


**Figure 1.** A small region of the KPNO, POLARBASE, and ELODIE spectra of HD 218209 and the Sun. Identified lines are also indicated.

## 2. OBSERVATIONS

For the creation of the line list in this study, high resolution ( $R \approx 42\,000$ ) and high signal to noise ( $S/N = 165$  at 550 nm) ELODIE spectrum (HJD 2451184.23521;  $R \approx 42\,000$ ; exposure time 1800 s) of HD 218209 was selected. The ELODIE cross-dispersed echelle spectrograph provided spectral coverage from 3900 to 6800 Å. The spectrum was continuum normalized and wavelength calibrated, and the radial velocity (RV) was corrected by the data reduction pipeline at the telescope. Since some problems were encountered in the continuum normalization of the spectra from the library, the spectrum was renormalized.

Since high resolution ( $R \approx 76\,000$ ) and high signal to noise ( $S/N = 140$  at 550 nm) POLARBASE<sup>1</sup> (Petit et al. 2014) Narval<sup>2</sup> spectrum (HJD 2456232.48238; exposure time 400 s) of the star was also available, it was used to test model parameters for the star. Prior to the line measurement process, the POLARBASE spectrum was also renormalized and corrected for the radial velocity (RV). For RV correction, we used a Python interface and the NARVAL atomic line library containing atomic transitions from 4000 to 6800 Å. For renormalization, we used an in-house developed interactive normalization code LIME (Şahin 2017) in Interactive Data Language (IDL) prior to the abundance analysis.

The Solar spectrum is certainly a primary reference for stellar astrophysics and for interpreting physical processes in stars (Molaro & Monai 2012). The high-resolution ( $R \approx 400\,000$ ) spectrum of the Sun used in this study was obtained with the Kitt Peak Fourier Transform Spectrometer (FTS; Kurucz et al. 1984). The character of the spectra of HD 218209 and the Sun is displayed in Figure 1.

<sup>1</sup> <http://polarbase.irap.omp.eu>

<sup>2</sup> Narval spectropolarimeter is adapted to the 2m Bernard Lyot telescope and provides high-resolution spectral and polarimetric data.

### 3. THE ABUNDANCE ANALYSIS

We employed ATLAS9 model atmospheres (Castelli & Kurucz 2003) computed in local thermodynamic equilibrium (LTE) with NEWODF opacities for abundance study of HD 218209 and the Solar spectrum. Elemental abundances were computed by using the LTE line analysis code MOOG (Sneden 1973)<sup>3</sup>. The details of the abundance analysis and the source of the atomic data are the same as in Şahin & Lambert (2009), Şahin et al. (2011, 2016) and Şahin & Bilir (2020). The line list, atomic data, and model parameter derivation are covered in the following subsections.

#### 3.1. Line List: Line Measurement, Identification and Atomic Data

An essential prerequisite for abundance analysis of a star is a set of reliably identified lines with reliable atomic data. Our line lists were created by a systematic search for unblended lines (useful for equivalent width–EW–analysis technique). For line measurement from the ELODIE spectrum of HD 218209, a systematic search for unblended lines was performed. The line centre positions were measured in several segments, each containing a portion of the spectra of 20 Å. For this, the LIME (Şahin 2017) code was employed. The code provides a list of possible transitions in the close neighbourhood of the measured line together with recent atomic data (e.g. Rowland Multiplet Number-RMT,  $\log g f$ , and lower Level Excitation Potential-LEP) that are compiled from the literature (e.g. from NIST database). The MOORE catalogue (Moore et al. 1966) was configured as one of the reference atomic line libraries in the LIME code. Following the line identification step, a multiplet analysis technique was performed to assess whether the detected lines belong to the candidate element indicated by the code. Our final list covers 24 species and 363 lines over the spectrum range from about 4100 – 6800 Å. The identified lines have accurate  $g f$ -values and are free of blends in the spectra of the Sun and HD 218209. The number of identified lines in the respective wavelength regions of the KPNO Solar spectrum is presented in Figure 2. Our selection of iron lines included 132 Fe I lines with excitation potentials (LEPs) ranging from 0.05 to  $\approx 5$  eV and 17 Fe II lines. Chosen lines of Fe I and Fe II are exhibited in Table 1. In Table 2, we provide the list of identified lines other than iron with the atomic data, their measured equivalent widths (obtained using the LIME code) and computed logarithmic abundances in the Solar spectrum and in the spectrum of HD 218209.

Atomic data forms the basis for line diagnostics. During the calculation of element abundances, two basic atomic data stand out, namely the lower level excitation potential (LEP) and the oscillator strength ( $\log g f$ ). Since the LEP values are measured with great accuracy, the main source of errors in abundance analysis usually comes from the  $\log g f$  measurements. The sensitivity of the measurements to determine the  $\log g f$  values affects the sensitivity of the spectral analysis performed. This situation may lead to incorrect calculation of model atmosphere parameters. Astrophysical  $g f$ -values were avoided due to the model dependence of such a procedure. We calculated Solar abundances using stellar lines to assess the uncertainty in  $\log g f$ -values and to minimise systematic errors. The lines were measured from the Kurucz et al. (1984) Solar flux atlas and analysed with the Solar model atmosphere from the Castelli & Kurucz (2003) grid for  $T_{\text{eff}} = 5790$  K, and  $\log g = 4.4$  cgs. Our calculations yielded a microturbulent of  $0.7 \text{ km s}^{-1}$  and the Solar abundances shown in Table 3. As can be noticed, the Solar abundances were successfully replicated.

<sup>3</sup> The MOOG source code is available at <http://www.as.utexas.edu/chris/moog.html>

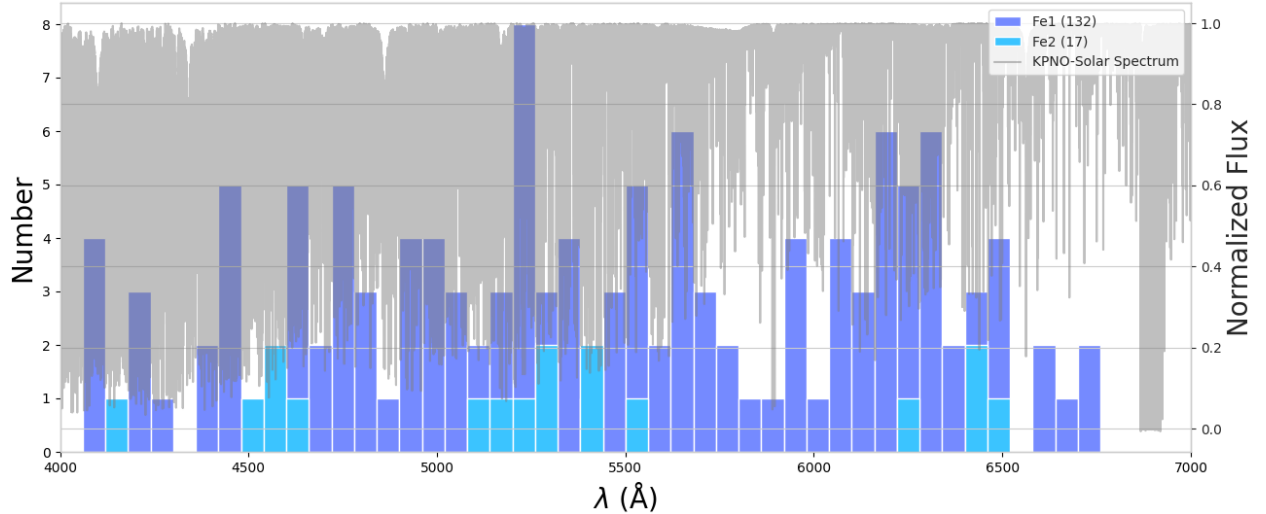


**Figure 2.** The KPNO Solar spectrum and the number of identified lines in the respective wavelength regions (each bar indicates 50 Å region of the spectrum).

We use our Solar abundances to compare stellar abundances to Solar abundances. As a result, the analysis in this study is done differently in relation to the Sun. Preference for a differential approach to analysis like this will reduce the errors caused by uncertainty in oscillator strengths, the influence of spectrograph features, and departures from LTE. Effective temperature errors in the spectroscopic excitation technique can also arise from systematic errors in oscillator strength as a function of excitation potential. The same holds true for errors with equivalent widths.

Further verification of the  $\log g f$  values was performed by comparing the  $\log g f$  values used in this study with those in the *Gaia-ESO* line list v.6 provided by the GES collaboration (Heiter et al. 2021). It should be noted that the  $g f$ -values for the chosen lines of Fe I and Fe II in this study were taken from the compilation of Fuhr & Wiese (2006). The GES line list contains a list of recommended lines and atomic data (hyperfine structure-has-corrected  $g f$ -values) for the analysis of FGK stars. It is worth noting that several lines in the spectra of FGK stars have not yet been identified (Heiter et al. 2015).

The GES line list (v.6) contains a total of 141 233 lines in the wavelength range 4200 – 10 000 Å. This number is reduced to 84 735 lines in the wavelength range 4200 - 6800 Å. For species that match those in the line list (24 in total) provided in this study in the same wavelength range, the GES contains 50 326 lines. This wavelength range is the same as the wavelength range for the ELODIE spectrum used for diagnostics. Comparing the GES line list with the new line list provided useful information. We used a total of 363 lines from the line list to match the GES lines. Out of 363 lines, 11 lines were found to be out of range ( $< 4200 \text{ \AA}$ ) in the GES line list and the two were missing (Y II lines at 4883.69 Å and 5087.43 Å). The search resulted in a one-to-one match of 350 lines in terms of wavelength, element,  $\log g f$  and low LEP. The difference between the  $\log g f$  values<sup>4</sup> for the 128 common Fe I lines in the GES line list was  $-0.03 \pm 0.06$  dex. For the 16 Fe II lines, the difference in  $\log g f$  values was  $-0.002 \pm 0.079$  dex. For, Na I, Si I, Ca I, Sc II, Ti I, Ti II, V I, Cr I, Ni I, Zn I, Sr I, Zr II, and Sm II, the difference in the  $\log g f$  values was less than 0.05 dex. For 54 common Ni I lines, the difference was found to be  $-0.045 \pm 0.114$  dex. A formal least square solution gives a gradient of 0.99 and a zero point difference of -0.02 dex over 350 common lines. However, there were large

<sup>4</sup>  $\log g f_{\text{This study}} - \log g f_{\text{GES}}$

**Table 1.** Fe I and Fe II lines. The abundances are obtained for a model of  $T_{\text{eff}} = 5790$  K,  $\log g = 4.4$  cgs, and  $\xi = 0.66$  km s $^{-1}$ .

Spec.	Sun						HD 218209						Sun						HD 218209					
	$\lambda$	LEP	$\log(gf)$	EW	$\log \epsilon(X)$		EW	$\log \epsilon(X)$	RMT	Spec.	$\lambda$	LEP	$\log(gf)$	EW	$\log \epsilon(X)$		EW	$\log \epsilon(X)$	RMT					
	(Å)	(eV)	(dex)	(mÅ)	(dex)		(mÅ)	(dex)			(Å)	(eV)	(dex)	(mÅ)	(dex)		(mÅ)	(dex)						
Fe I	4080.22	3.28	-1.23	80.9	7.34	85.1	7.16	558	Fe I	5618.64	4.21	-1.28	49.3	7.47	34.3	7.04	1107							
Fe I	4082.11	3.42	-1.51	72.7	7.60	69.8	7.34	698	Fe I	5624.03	4.39	-1.20*	49.2	7.55	38.9	7.22	1160							
Fe I	4088.56	3.64	-1.50	52.4	7.43	43.9	7.09	906	Fe I	5635.95	4.99	-0.32	67.3	7.62	53.2	7.23	1314							
Fe I	4090.96	3.37	-1.73	55.5	7.39	49.9	7.10	700	Fe I	5636.71	3.64	-2.56	19.6	7.51	13.0	7.18	868							
Fe I	4204.00	2.84	-1.01	125.1	7.52	115.9	7.14	355	Fe I	5638.27	4.22	-0.84	75.4	7.54	61.1	7.12	1087							
Fe I	4207.13	2.83	-1.41	83.5	7.44	88.1	7.31	352	Fe I	5641.45	4.26	-1.15	66.0	7.71	45.4	7.18	1087							
Fe I	4220.35	3.07	-1.31	91.4	7.63	70.9	7.01	482	Fe I	5662.52	4.18	-0.57	92.4	7.61	81.1	7.24	1087							
Fe I	4291.47	0.05	-4.08	92.3	7.51	87.1	7.12	3	Fe I	5701.56	2.56	-2.22	87.1	7.68	70.6	7.17	209							
Fe I	4365.90	2.99	-2.25	49.2	7.44	38.1	7.03	415	Fe I	5705.47	4.30	-1.36	37.5	7.38	25.8	7.01	1087							
Fe I	4389.25	0.05	-4.58	75.4	7.65	63.9	7.12	2	Fe I	5717.84	4.28	-1.10	63.3	7.62	53.8	7.29	1107							
Fe I	4432.58	3.57	-1.56	51.4	7.38	40.2	6.97	797	Fe I	5741.86	4.26	-1.67	31.5	7.51	21.8	7.18	1086							
Fe I	4439.89	2.28	-3.00	48.4	7.49	34.4	6.99	116	Fe I	5778.46	2.59	-3.43	21.5	7.41	13.6	7.03	209							
Fe I	4442.35	2.20	-1.25	187.7	7.54	167.6	7.09	68	Fe I	5806.73	4.61	-1.03	56.4	7.69	39.7	7.25	1180							
Fe I	4447.14	2.20	-2.73	66.2	7.66	64.1	7.45	69	Fe I	5916.26	2.45	-2.99	54.5	7.62	40.7	7.17	170							
Fe I	4447.73	2.22	-1.34	171.0	7.54	155.7	7.11	68	Fe I	5929.68	4.55	-1.38	39.7	7.66	28.6	7.32	1176							
Fe I	4502.60	3.57	-2.31	28.9	7.53	29.1	7.44	796	Fe I	5934.67	3.93	-1.12	76.6	7.47	61.7	7.05	982							
Fe I	4556.93	3.25	-2.66	25.9	7.48	12.7	6.95	638	Fe I	5952.73	3.98	-1.39	59.6	7.50	53.0	7.22	959							
Fe I	4593.53	3.94	-2.03	28.3	7.54	16.1	7.10	971	Fe I	5956.71	0.86	-4.61	52.8	7.62	—	—	14							
Fe I	4602.01	1.61	-3.15	72.0	7.58	64.8	7.21	39	Fe I	6027.06	4.07	-1.09	62.7	7.48	48.8	7.05	1018							
Fe I	4602.95	1.48	-2.22	122.5	7.51	116.3	7.13	39	Fe I	6065.49	2.61	-1.53	118.5	7.45	102.9	7.00	207							
Fe I	4619.30	3.60	-1.08	84.1	7.45	73.7	7.06	821	Fe I	6079.02	4.65	-1.10	45.6	7.59	34.8	7.26	1176							
Fe I	4630.13	2.28	-2.59	72.7	7.63	61.9	7.19	115	Fe I	6082.72	2.22	-3.57	35.2	7.52	28.1	7.21	64							
Fe I	4635.85	2.84	-2.36	54.9	7.54	41.2	7.06	349	Fe I	6096.67	3.98	-1.88	37.5	7.55	27.2	7.22	959							
Fe I	4678.85	3.60	-0.83	102.5	7.47	95.2	7.13	821	Fe I	6127.91	4.14	-1.40	48.3	7.52	37.3	7.17	1017							
Fe I	4704.95	3.69	-1.53	61.5	7.55	48.6	7.12	821	Fe I	6137.70	2.59	-1.40	135.6	7.48	122.8	7.07	207							
Fe I	4728.55	3.65	-1.17	81.3	7.65	69.3	7.23	822	Fe I	6157.73	4.07	-1.22	61.0	7.56	53.2	7.26	1015							
Fe I	4733.60	1.48	-2.99	82.9	7.58	84.8	7.40	38	Fe I	6165.36	4.14	-1.47	44.6	7.51	30.7	7.09	1018							
Fe I	4735.85	4.07	-1.32	64.1	7.79	57.6	7.50	1042	Fe I	6173.34	2.22	-2.88	68.9	7.61	58.6	7.22	62							
Fe I	4741.53	2.83	-1.76	72.6	7.41	63.5	7.03	346	Fe I	6180.21	2.73	-2.65	53.4	7.52	47.6	7.25	269							
Fe I	4745.81	3.65	-1.27	78.2	7.69	66.2	7.27	821	Fe I	6200.32	2.61	-2.44	71.5	7.59	62.6	7.23	207							
Fe I	4788.77	3.24	-1.76	65.6	7.61	55.0	7.20	588	Fe I	6213.44	2.22	-2.48	82.5	7.50	75.6	7.18	62							
Fe I	4802.89	3.64	-1.51	60.0	7.52	44.3	7.02	888	Fe I	6219.29	2.20	-2.43	87.9	7.54	79.1	7.18	62							
Fe I	4839.55	3.27	-1.82	62.2	7.60	58.3	7.37	588	Fe I	6232.65	3.65	-1.22	81.5	7.60	71.9	7.25	816							
Fe I	4875.88	3.33	-1.97	61.0	7.60	49.2	7.20	687	Fe I	6240.65	2.22	-3.17	47.6	7.40	39.1	7.06	64							
Fe I	4917.23	4.19	-1.16	62.7	7.61	49.4	7.21	1066	Fe I	6252.56	2.40	-1.69	119.6	7.42	103.2	6.96	169							
Fe I	4918.02	4.23	-1.34	53.0	7.63	45.5	7.35	1070	Fe I	6265.14	2.18	-2.55	86.2	7.60	82.5	7.33	62							
Fe I	4924.78	2.28	-2.11	92.8	7.52	85.2	7.15	114	Fe I	6270.23	2.86	-2.61	53.0	7.58	43.1	7.23	342							
Fe I	4939.69	0.86	-3.34	99.7	7.58	95.8	7.24	16	Fe I	6297.80	2.22	-2.74	73.6	7.56	67.1	7.26	62							
Fe I	4961.92	3.63	-2.25	26.5	7.42	16.4	7.03	845	Fe I	6301.51	3.65	-0.72	112.7	7.57	106.2	7.26	816							
Fe I	4962.58	4.18	-1.18	54.0	7.51	40.3	7.09	66	Fe I	6315.81	4.07	-1.66	39.8	7.51	—	—	1014							
Fe I	4973.10	3.96	-0.92	93.8	7.72	82.4	7.34	173	Fe I	6322.69	2.59	-2.43	78.6	7.69	61	7.16	207							
Fe I	5002.80	3.40	-1.53	78.8	7.54	81.2	7.35	687	Fe I	6335.34	2.20	-2.18	96.3	7.43	88.6	7.08	62							
Fe I	5022.24	3.98	-0.56	99.5	7.45	93.9	7.14	965	Fe I	6336.83	3.69	-0.86	102.4	7.34	94.8	7.01	816							
Fe I	5029.62	3.41	-2.00	48.7	7.54	40.0	7.21	718	Fe I	6344.15	2.43	-2.92	59.2	7.61	56.4	7.40	169							
Fe I	5074.75	4.22	-0.23	118.8	7.50	105.8	7.12	1094	Fe I	6393.61	2.43	-1.58	134.6	7.48	113.4	6.99	168							
Fe I	5083.35	0.96	-2.96	109.9	7.43	101.8	7.02	16	Fe I	6408.03	3.69	-1.02	97.3	7.69	88.1	7.35	816							
Fe I	5088.16	4.15	-1.75	34.8	7.59	23.5	7.22	1066	Fe I	6419.96	4.73	-0.27	86.8	7.51	71.3	7.11	1258							
Fe I	5141.75	2.42	-2.24	89.3	7.68	76.5	7.23	114	Fe I	6430.86	2.18	-2.01	115.3	7.51	97.9	7.03	62							
Fe I	5145.10	2.20	-3.08*	52.5	7.49	49.0	7.26	66	Fe I	6469.19	4.83	-0.81	58.6	7.68	44.5	7.31	1258							
Fe I	5198.72	2.22	-2.13	94.9	7.48	91.1	7.17	66	Fe I	6481.88	2.28	-2.98	64.7	7.63	62.9	7.44	109							
Fe I	5217.40	3.21	-1.16	121.7	7.52	93.8	6.94	553	Fe I	6498.94	0.96	-4.69	45.7	7.59	40.9	7.32	13							
Fe I	5228.38	4.22	-1.26	60.0	7.68	53.5	7.41	1091	Fe I	6518.37	2.83	-2.46†	56.0	7.46	—	—	342							
Fe I	5242.50	3.63	-0.97	85.7	7.50	73.2	7.08	843	Fe I	6593.88	2.43	-2.42	83.7	7.60	75.0	7.25	168							
Fe I	5243.78	4.26	-1.12	63.0	7.64	46.6	7.18	1089	Fe I	6609.12	2.56	-2.69	65.6	7.62	55.1	7.25	206							
Fe I	5247.06	0.09	-4.95	65.3	7.58	61.3	7.30	1	Fe I	6678.00	2.69	-1.42	133.5	7.54	112.1	7.05	268							
Fe I	5250.22	0.12	-4.94	65.9	7.62	61.5	7.32	1	Fe I	6703.58	2.76	-3.06	37.2	7.55	31.7	7.3	268							
Fe I	5250.65	2.20	-2.18	100.6	7.60	95.7	7.27	66	Fe I	6750.16	2.42	-2.62	73.3	7.56	61.8	7.16	111							
Fe I	5253.47	3.28	-1.57	77.9	7.42	62.2	6.94	553	Fe I	6781.86	2.58	-2.51*	89.7	7.50	77.2	7.19	28							
Fe I	5288.53	3.69	-1.51	58.6	7.52	48.4	7.15	929	Fe I	6508.29	2.85	-2.44*	82.1	7.46	76.6	7.30	38							
Fe I	5298.78	3.64	-2.02	42.2	7.57	30.3	7.18	875	Fe I	6576.34	2.84	-2.												

# An Up to Date Line List for Spectroscopic Analysis of F and G Stars

**Table 2.** Lines used in the analysis of the KPNO Solar spectrum and HD 218209. Abundances for individual lines are those obtained for a model of  $T_{\text{eff}} = 5790$  K,  $\log g = 4.4$  cgs, and  $\xi = 0.66$  km s $^{-1}$ .

Spec.	Sun						HD 218209						Sun						HD 218209	
	$\lambda$ (Å)	LEP (eV)	$\log(gf)$ (dex)	EW (mÅ)	$\log \epsilon(X)$ (dex)	EW (mÅ)	$\log \epsilon(X)$ (dex)	RMT	Ref.	Spec.	$\lambda$ (Å)	LEP (eV)	$\log(gf)$ (dex)	EW (mÅ)	$\log \epsilon(X)$ (dex)	EW (mÅ)	$\log \epsilon(X)$ (dex)	RMT	Ref.	
Na I	5682.65	2.10	-0.67	100.1	6.21	82.4	5.86	6	1	Ti I	5145.47	1.46	-0.54	37.2	4.94	31.4	4.67	109	7	
Na I	5688.22	2.10	-0.37	121.1	6.11	99.9	5.72	6	1	Ti I	5147.48	0.00	-1.94	38.8	4.93	37.7	4.73	4	7	
Mg I	4571.10	0.00	-5.40	109.2	7.54	115.1	7.44	1	2	Ti I	5152.19	0.02	-1.95	36.9	4.92	—	—	4	7	
Mg I	5711.10	4.34	-1.74	104.6	7.65	107.6	7.52	8	2	Ti I	5192.98	0.02	-0.95	84.0	5.03	85.2	4.83	4	7	
Si I	5645.62	4.93	-2.03	35.5	7.50	—	—	10	3	Ti I	5210.39	0.05	-0.82	89.0	5.03	98.6	4.95	4	7	
Si I	5665.56	4.92	-1.99	39.6	7.53	31.0	7.37	10	3	Ti I	5219.71	0.02	-2.22	29.1	5.00	29.0	4.82	4	7	
Si I	5684.49	4.95	-1.58	60.6	7.52	54.3	7.35	11	3	Ti I	5490.16	1.46	-0.84	22.4	4.85	25.6	4.80	3	7	
Si I	5708.40	4.95	-1.47	74.7	7.64	62.2	7.37	10	4	Ti I	5866.46	1.07	-0.79	46.9	4.97	44.9	4.78	72	7	
Si I	5772.15	5.08	-1.62	52.0	7.53	40.0	7.27	17	3	Ti I	6126.22	1.07	-1.42	21.7	5.00	23.0	4.88	69	7	
Si I	5793.08	4.93	-1.86	42.4	7.46	31.6	7.20	9	3	Ti I	6258.11	1.44	-0.39	51.4	5.00	48.3	4.78	104	7	
Si I	5948.54	5.08	-1.09	83.8	7.51	—	—	16	3	Ti I	6261.11	1.43	-0.53	49.9	5.10	53.2	5.02	104	7	
Si I	6125.03	5.61	-1.53	30.9	7.51	23.1	7.31	30	3	Ti I	6336.11	1.44	-1.69	5.60	4.92	—	—	103	7	
Si I	6142.49	5.62	-1.48	33.3	7.51	26.8	7.35	30	3	Ti I	6743.13	0.90	-1.63	18.0	4.89	—	—	48	7	
Si I	6145.02	5.61	-1.39	37.9	7.50	27.6	7.26	29	3	Ti II	4443.81	1.08	-0.71	139.7	5.04	139.9	4.86	19	7	
Si I	6244.48	5.61	-1.29	44.0	7.51	32.9	7.27	27	3	Ti II	4468.50	1.13	-0.63	134.1	4.94	149.8	4.90	31	7	
Si I	6721.84	5.86	-0.94	42.3	7.33	29.1	7.06	38*	4	Ti II	4493.53	1.08	-2.78	34.2	4.90	40.1	5.01	18	7	
Ca I	4512.27	2.52	-1.90	25.0	6.33	16.3	5.99	24	5	Ti II	4568.33	1.22	-2.65	32.0	4.84	26.7	4.68	60	7	
Ca I	4578.56	2.52	-0.70	85.8	6.33	89.4	6.18	23	5	Ti II	4583.41	1.16	-2.84	31.7	4.96	25.6	4.77	39	7	
Ca I	5260.39	2.52	-1.72	33.2	6.32	25.2	6.04	22	5	Ti II	4708.67	1.24	-2.35	51.0	5.02	44.0	4.82	49	7	
Ca I	5261.71	2.52	-0.58	98.7	6.49	91.7	6.19	22	5	Ti II	4874.01	3.09	-0.86	36.4	4.91	27.3	4.70	114	7	
Ca I	5512.99	2.93	-0.46	83.9	6.36	82.2	6.16	48	5	Ti II	4911.20	3.12	-0.64	51.4	5.11	48.7	5.06	114	7	
Ca I	5581.98	2.52	-0.56	94.3	6.38	88.8	6.11	21	5	Ti II	5005.17	1.57	-2.73	23.9	5.02	16.2	4.76	71	7	
Ca I	5590.13	2.52	-0.57	93.0	6.37	86.6	6.09	21	5	Ti II	5013.69	1.58	-2.14	49.5	5.08	43.7	4.92	71	7	
Ca I	5601.29	2.52	-0.52	102.8	6.47	99.0	6.21	21	5	Ti II	5336.79	1.58	-1.60	72.3	5.09	71.0	5.03	69	7	
Ca I	6102.73	1.88	-0.81	122.3	6.10	123.8	5.86	3	5	Ti II	5418.77	1.58	-2.13	48.7	5.02	41.3	4.83	69	7	
Ca I	6166.44	2.52	-1.14	72.3	6.37	64.2	6.08	20	5	V I	4437.84	0.29	-0.71	37.1	4.03	32.9	3.76	21	8	
Ca I	6169.04	2.52	-0.80	93.5	6.34	90.8	6.09	20	5	V I	4577.18	0.00	-1.08	33.6	4.01	36.5	3.91	4	8	
Ca I	6169.56	2.52	-0.48	114.0	6.26	109.4	5.98	20	5	V I	5727.06	1.08	-0.02	38.7	4.04	—	—	35	8	
Ca I	6455.60	2.52	-1.34	56.7	6.39	47.3	6.09	19	5	V I	6119.53	1.06	-0.36	22.1	3.93	21.8	3.78	34	8	
Ca I	6471.67	2.52	-0.69	89.3	6.35	85.2	6.12	18	5	V I	6243.11	0.30	-0.94	29.6	3.94	29.9	3.78	19	8	
Ca I	6493.79	2.52	-0.11	124.4	6.26	116.6	5.95	18	5	Cr I	4545.96	0.94	-1.38	81.6	5.68	80.4	5.43	10	4	
Ca I	6499.65	2.52	-0.82	82.5	6.37	81.2	6.19	18	5	Cr I	4616.13	0.98	-1.18	90.3	5.71	83.3	5.34	21	4	
Ca I	6572.79	0.00	-4.32	32.1	6.37	33.4	6.24	1	5	Cr I	4626.18	0.97	-1.32	82.2	5.66	72.7	5.24	21	4	
Ca I	6717.69	2.71	-0.52	99.5	6.36	98.7	6.04	32	5	Cr I	4646.17	1.03	-0.71	105.5	5.55	94.3	5.11	21	4	
Sc I	4023.69	0.02	0.38	57.5	3.12	51.3	2.78	7	6	Cr I	4651.29	0.98	-1.46	82.9	5.82	66.1	5.23	21	4	
Sc II	4246.84	0.31	0.24	156.6	3.17	153.8	2.94	7	6	Cr I	4652.17	1.00	-1.03	100.8	5.77	86.3	5.26	21	4	
Sc II	5239.82	1.45	-0.76	52.0	3.22	48.7	3.12	26	6	Cr I	4708.02	3.17	0.11	57.5	5.58	41.5	5.11	186	4	
Sc II	5526.82	1.77	-0.01	75.1	3.32	65.4	3.06	31	6	Cr I	4718.42	3.19	0.10	64.1	5.74	55.9	5.42	186	4	
Sc II	5640.99	1.50	-0.99	39.7	3.18	34.7	3.04	29	6	Cr I	4730.72	3.08	-0.19	48.3	5.67	30.5	5.12	145	4	
Sc II	5657.88	1.51	-0.54	66.1	3.36	55.6	3.09	29	6	Cr I	4737.35	3.07	-0.10	55.7	5.68	43.0	5.26	145	4	
Sc II	5667.15	1.50	-1.21	32.1	3.22	26.1	3.05	29	6	Cr I	4756.12	3.10	0.09	62.9	5.76	52.3	5.39	145	4	
Sc II	5669.04	1.50	-1.10	34.1	3.16	29.7	3.03	29	6	Cr I	4936.34	3.11	-0.34	46.2	5.77	37.6	5.46	166	4	
Ti I	4060.27	1.05	-0.69	37.8	4.82	44.5	4.83	80	7	Cr I	4964.93	0.94	-2.53	37.7	5.65	33.3	5.40	9	4	
Ti I	4186.13	1.50	-0.24	42.7	4.91	43.7	4.79	129	7	Cr I	5247.57	0.96	-1.63	82.0	5.78	74.5	5.42	18	4	
Ti I	4287.41	0.84	-0.37	75.3	5.20	76.7	5.01	44	7	Cr I	5296.70	0.98	-1.41	91.9	5.77	80.7	5.33	18	4	
Ti I	4453.32	1.43	-0.03	64.5	5.16	—	—	113	7	Cr I	5300.75	0.98	-2.13	58.6	5.75	44.0	5.25	18	4	
Ti I	4465.81	1.74	-0.13	40.9	4.95	40.7	4.81	146	7	Cr I	5345.81	1.00	-0.98	116.8	5.73	111.0	5.37	18	4	
Ti I	4512.74	0.84	-0.40	67.5	4.99	68.4	4.82	42	7	Cr I	5348.33	1.00	-1.29	99.5	5.79	86.5	5.32	18	4	
Ti I	4518.03	0.83	-0.25	73.0	4.97	74.6	4.80	42	7	Cr I	5787.93	3.32	-0.08	45.7	5.62	32.3	5.22	188	4	
Ti I	4534.79	0.84	0.35	95.9	4.86	96.5	4.60	42	7	Cr II	4588.20	4.07	-0.65	71.8	5.69	59.4	5.40	44	9	
Ti I	4548.77	0.83	-0.28	70.9	4.95	82.8	4.99	42	7	Cr II	5237.32	4.07	-1.17	53.0	5.75	39.2	5.42	43	9	
Ti I	4555.49	0.85	-0.40	63.1	4.89	64.5	4.74	42	7	Cr II	5305.87	3.83	-1.91	24.6	5.48	13.2	5.13	24	9	
Ti I	4617.28	1.75	0.44	63.7	4.94	61.3	4.72	145	7	Mn I	4055.55	2.14	-0.08	125.5	5.76	107.2	5.26	5	10	
Ti I	4623.10	1.74	0.16	56.6	5.03	52.7	4.79	145	7	Mn I	4082.94	2.18	-0.36	91.3	5.60	76.6	5.07	5	10	
Ti I	4639.36	1.74	-0.05	43.2	4.90	49.4	4.91	145	7	Mn I	4451.59	2.89	0.28	95.1	5.55	80.0	5.06	22	10	
Ti I	4639.66	1.75	-0.14	43.5	5.01	44.4	4.89	145	7	Mn I	4470.14	2.94	-0.44	56.9	5.46	36.7	4.82	22	10	
Ti I	4656.47	0.00	-1.28	68.8	5.07	76.2	5.05	6	7	Mn I	4502.22	2.92	-0.34	59.6	5.41	43.1	4			

**Table 2 continued**

Spec.	Sun						HD 218209						Sun						HD 218209					
	$\lambda$ (Å)	LEP (eV)	$\log(gf)$ (dex)	EW (mÅ)	$\log \epsilon(X)$ (dex)	EW (mÅ)	$\log \epsilon(X)$ (dex)	RMT	Ref.	Spec.	$\lambda$ (Å)	LEP (eV)	$\log(gf)$ (dex)	EW (mÅ)	$\log \epsilon(X)$ (dex)	EW (mÅ)	$\log \epsilon(X)$ (dex)	RMT	Ref.					
Ni I	4410.52	3.31	-1.08	57.8	6.39	43.1	5.94	88	4	Ni I	5748.36	1.68	-3.26	28.8	6.26	19.3	5.87	45	4					
Ni I	4470.48	3.40	-0.40	79.5	6.24	76.2	5.98	86	4	Ni I	5805.23	4.17	-0.64	40.5	6.30	28.2	5.93	234	4					
Ni I	4606.23	3.60	-1.02	48.0	6.37	38.8	6.05	100	4	Ni I	6007.32	1.68	-3.34	25.4	6.24	22.5	6.04	42	4					
Ni I	4686.22	3.60	-0.64	62.3	6.30	58.9	6.08	98	4	Ni I	6086.29	4.26	-0.51	43.5	6.30	28.2	5.88	249	4					
Ni I	4731.80	3.83	-0.85	45.4	6.35	26.6	5.82	163	4	Ni I	6108.12	1.68	-2.44	65.6	6.30	55.3	5.92	45	4					
Ni I	4732.47	4.10	-0.55	44.3	6.29	30.6	5.89	235	4	Ni I	6128.98	1.68	-3.32	25.3	6.21	20.1	5.94	42	4					
Ni I	4752.43	3.66	-0.69	59.1	6.33	43.1	5.86	132	4	Ni I	6130.14	4.26	-0.96	21.6	6.24	11.5	5.82	248	4					
Ni I	4756.52	3.48	-0.34	77.5	6.19	76.1	5.96	98	4	Ni I	6175.37	4.09	-0.54	50.7	6.32	36.4	5.92	217	4					
Ni I	4806.99	3.68	-0.64	61.4	6.35	54.7	6.07	163	4	Ni I	6176.82	4.09	-0.53	63.0	6.54	48.0	6.13	228	4					
Ni I	4829.03	3.54	-0.33	80.1	6.24	68.7	5.85	131	4	Ni I	6204.61	4.09	-1.14	21.7	6.26	18.2	6.08	226	4					
Ni I	4852.56	3.54	-1.07	44.7	6.28	42.3	6.10	130	4	Ni I	6322.17	4.15	-1.17	18.3	6.24	—	—	249	4					
Ni I	4904.42	3.54	-0.17	87.1	6.19	78.1	5.84	129	4	Ni I	6327.60	1.68	-3.15	37.9	6.34	27.8	5.97	44	4					
Ni I	4913.98	3.74	-0.62	55.3	6.24	42.3	5.84	132	4	Ni I	6378.26	4.15	-0.90	31.5	6.32	23.5	6.04	247	4					
Ni I	4935.83	3.94	-0.36	62.9	6.30	48.5	5.88	177	4	Ni I	6414.59	4.15	-1.21	16.8	6.23	—	—	244	4					
Ni I	4946.03	3.80	-1.29	28.0	6.35	17.0	5.96	148	4	Ni I	6482.81	1.93	-2.63	40.8	6.12	31.8	5.79	66	4					
Ni I	4953.21	3.74	-0.66	56.2	6.30	40.9	5.85	111	4	Ni I	6598.61	4.23	-0.98	24.7	6.30	—	—	249	4					
Ni I	4998.23	3.61	-0.78	57.5	6.33	43.2	5.90	111	4	Ni I	6635.14	4.42	-0.83	24.0	6.31	15.2	5.97	264	4					
Ni I	5010.94	3.63	-0.87	48.4	6.23	33.4	5.79	144	4	Ni I	6767.78	1.83	-2.17	79.6	6.47	67.4	6.06	57	4					
Ni I	5032.73	3.90	-1.27	23.8	6.31	16.2	6.00	207	4	Ni I	6772.32	3.66	-0.99	48.4	6.27	35.3	5.89	127	4					
Ni I	5035.37	3.63	0.29	107.0	6.05	91.5	5.63	143	4	Zn I	4722.16	4.03	-0.39	66.1	4.70	65.0	4.58	2	12					
Ni I	5042.19	3.64	-0.57	61.8	6.21	52.6	5.88	131	4	Zn I	4810.54	4.08	-0.17	72.3	4.66	73.6	4.58	2	12					
Ni I	5048.85	3.85	-0.37	66.1	6.29	51.5	5.86	195	4	Sr I	4607.34	0.00	0.28	45.4	2.91	32.0	2.28	2	13					
Ni I	5082.35	3.66	-0.54	62.5	6.22	55.2	5.92	130	4	Y II	4883.69	1.08	0.07	57.6	2.33	53.4	2.15	22	14					
Ni I	5084.10	3.68	0.03	91.1	6.14	78.2	5.75	162	4	Y II	5087.43	1.08	-0.17	48.3	2.25	31.1	1.69	20	14					
Ni I	5088.54	3.85	-0.91	31.9	6.12	23.9	5.83	190	4	Zr II	4208.98	0.71	-0.46	44.7	2.68	39.3	2.45	41	15					
Ni I	5102.97	1.68	-2.62	48.1	6.16	36.7	5.74	49	4	Ba II	4554.04	0.00	0.14	174.6	2.17	154.7	1.78	1	16					
Ni I	5115.40	3.83	-0.11	75.2	6.19	68.9	5.90	177	4	Ba II	5853.69	0.60	-0.91	62.8	2.28	51.2	1.87	2	16					
Ni I	5155.13	3.90	-0.66	49.2	6.28	34.5	5.86	206	4	Ba II	6141.71	0.70	-0.03	112.2	2.23	98.9	1.87	2	16					
Ni I	5435.87	1.99	-2.60	52.0	6.52	40.0	6.09	70	4	Ba II	6496.91	0.60	-0.41	97.5	2.30	90.6	2.01	2	16					
Ni I	5587.87	1.93	-2.14	55.8	6.08	39.7	5.56	70	4	Ce II	4562.37	0.48	0.21	21.9	1.65	18.6	1.47	1	17					
Ni I	5593.75	3.90	-0.84	45.4	6.35	28.3	5.88	206	4	Ce II	4628.16	0.52	0.14	18.4	1.63	12.9	1.34	1	17					
Ni I	5625.33	4.09	-0.70	38.1	6.24	28.8	5.94	221	4	Nd II	4446.40	0.20	-0.35	12.7	1.41	8.0	1.08	49	18					
Ni I	5637.12	4.09	-0.80	33.3	6.23	—	—	218	4	Nd II	5092.80	0.38	-0.61	7.0	1.48	—	—	48	18					
Ni I	5641.89	4.10	-1.08	24.6	6.31	13.1	5.87	234	4	Nd II	5293.17	0.82	0.10	10.3	1.39	—	—	75	18					
Ni I	5682.21	4.10	-0.47	51.9	6.30	33.9	5.83	232	4	Sm II	4577.69	0.25	-0.65	5.2	0.96	—	—	23	19					

References for the adopted  $gf$ -values: (1) Takeda et al. (2003), (2) Pehlivan Rhodin et al. (2017), (3) Shi et al. (2011), (4) NIST Atomic Spectra Database (<http://physics.nist.gov/PhysRefData/ASD>), (5) Den Hartog et al. (2021), (6) Lawler et al. (2019), (7) Lawler et al. (2013), (8) Lawler et al. (2014), (9) Lawler et al. (2017), (10) Den Hartog et al. (2011), (11) Lawler et al. (2015), (12) Biemont & Godefroid (1980), (13) Hansen et al. (2013), (14) Hannaford et al. (1982), (15) Biemont et al. (1981), (16) Klose et al. (2002), (17) Lawler et al. (2009), (18) Den Hartog et al. (2003), (19) Lawler et al. (2006), (†) Bard & Kock (1994), (\*) Meléndez & Barbuy (2009)

# An Up to Date Line List for Spectroscopic Analysis of F and G Stars

**Table 3.** Solar abundances obtained by employing the Solar model atmosphere from [Castelli & Kurucz \(2003\)](#) compared to the photospheric abundances from [Asplund et al. \(2009\)](#). The abundances were calculated using the line EWs.

Species	HD 218209				Sun <sup>†</sup>		<a href="#">Asplund et al. (2009)</a>	
	$\log \epsilon(X)^1$ (dex)	[X/Fe] <sup>1</sup> (dex)	[X/Fe] <sup>2</sup> (dex)	$N^1$	$\log \epsilon_{\odot}(X)$	$N$	$\log \epsilon_{\odot}(X)$ (dex)	$\Delta \log \epsilon_{\odot}(X)$
Na I	5.79±0.09	-0.02±0.14	0.00±0.18	2	6.16±0.07	2	6.24±0.04	0.08
Mg I	7.48±0.06	0.23±0.13	0.09±0.20	2	7.60±0.08	2	7.60±0.04	0.00
Si I	7.28±0.09	0.13±0.14	0.13±0.19	11	7.50±0.07	12	7.51±0.03	0.01
Ca I	6.09±0.10	0.10±0.15	0.10±0.19	18	6.34±0.08	18	6.34±0.04	0.00
Sc I	2.78±0.00	0.01±0.08	-0.33±0.14	1	3.12±0.00	1	3.15±0.04	0.03
Sc II	3.05±0.06	0.17±0.13	0.18±0.20	7	3.23±0.08	7	3.15±0.04	0.08
Ti I	4.82±0.12	0.21±0.17	0.21±0.21	39	4.96±0.09	43	4.95±0.05	0.01
Ti II	4.86±0.13	0.22±0.17	0.18±0.19	12	4.99±0.08	12	4.95±0.05	0.04
V I	3.81±0.07	0.17±0.12	0.05±0.15	4	3.99±0.05	5	3.93±0.08	0.06
Cr I	5.30±0.11	-0.06±0.15	-0.01±0.18	19	5.71±0.07	19	5.64±0.04	0.07
Cr II	5.32±0.16	0.03±0.23	-0.01±0.20	3	5.64±0.14	3	5.64±0.04	0.00
Mn I	5.06±0.15	-0.21±0.21	-0.23±0.23	12	5.62±0.13	13	5.43±0.05	0.19
Fe I	7.17±0.12	-0.02±0.17	-0.01±0.20	128	7.54±0.09	132	7.50±0.04	0.04
Fe II	7.16±0.07	0.00±0.11	0.00±0.19	15	7.51±0.04	17	7.50±0.04	0.01
Co I	4.62±0.15	0.00±0.23	0.03±0.26	6	4.97±0.15	7	4.99±0.07	0.02
Ni I	5.91±0.12	-0.02±0.17	-0.03±0.21	50	6.28±0.09	54	6.22±0.04	0.06
Zn I	4.58±0.01	0.25±0.09	0.26±0.17	2	4.68±0.03	2	4.56±0.05	0.12
Sr I	2.28±0.00	-0.28±0.08	-0.16±0.14	1	2.91±0.00	1	2.87±0.07	0.04
Y II	1.92±0.32	-0.02±0.33	-0.15±0.22	2	2.29±0.05	2	2.21±0.05	0.08
Zr II	2.45±0.00	0.12±0.08	0.27±0.14	1	2.68±0.00	1	2.58±0.04	0.10
Ba II	1.88±0.09	-0.01±0.13	0.06±0.20	4	2.24±0.06	4	2.18±0.09	0.06
Ce II	1.40±0.09	0.11±0.12	0.25±0.21	2	1.64±0.02	2	1.58±0.04	0.06
Nd II	1.08±0.00	0.01±0.09	0.19±0.14	1	1.42±0.05	3	1.42±0.04	0.00
Sm II	–	–	–	–	0.96±0.00	1	0.96±0.04	0.00

(1) The abundances are obtained using the ELODIE spectrum. (2) The abundances are obtained using the POLARBASE spectrum. (\*)  $\Delta \log \epsilon_{\odot}(X) = \log \epsilon_{\odot}(X)_{\text{This study}} - \log \epsilon_{\odot}(X)_{\text{Asplund}}$ . (†) The Solar abundances calculated in this study.

discrepancies in the  $\log g f$  values for transitions for some elements common to both line lists. Details about this discrepancy are included in the following section.

## 3.2. Model Parameters and Abundances

We used neutral and ionised Fe lines to determine model atmospheric parameters such as effective temperature, surface gravity, microturbulence, and metallicity (Table 4). First, the effective temperature was calculated by requiring that the resulting abundance be independent of the lower LEP.

If all lines have the same LEP and a similar wavelength, the microturbulence ( $\xi$ ) is determined by requiring that the calculated abundance be independent of the reduced equivalent width (EW). The precision in the determination of the microturbulent velocity is  $\pm 0.5 \text{ km s}^{-1}$ . We calculated surface gravity ( $\log g$ ) by requiring

**Table 4.** Model atmosphere parameters for HD 218209 and the Sun.

Star	$T_{\text{eff}}$ (K)	$\log g$ (cgs)	[Fe/H] (dex)	$\xi$ ( $\text{km s}^{-1}$ )
HD 218209 <sup>†</sup>	$5650^{+165}_{-170}$	$4.55^{+0.18}_{-0.21}$	$-0.35^{+0.07}_{-0.07}$	$0.60^{+0.50}_{-0.50}$
HD 218209 <sup>*</sup>	$5630^{+170}_{-160}$	$4.43^{+0.22}_{-0.26}$	$-0.31^{+0.13}_{-0.13}$	$0.35^{+0.50}_{-0.50}$
Sun	$5790^{+125}_{-125}$	$4.40^{+0.16}_{-0.23}$	$0.00^{+0.04}_{-0.04}$	$0.66^{+0.50}_{-0.50}$

(†) The ELODIE spectrum was used.

(\*) The PolarBase spectrum was used.

ionisation equilibrium, which means that the Fe I and Fe II lines yield the same iron abundance (Figures 3 and 4). Due to the interdependence of model parameters, an iterative procedure is required. Between each of the above steps, minor adjustments are made to the model parameters. We also confirmed that there is no substantial trend in iron abundances (see Figures 3 and 4 for the Sun and HD 218209, respectively).

The model parameters obtained for the Sun as a result of the Solar analysis were determined as  $T_{\text{eff}} = 5790$  K,  $\log g = 4.4$  cgs,  $[\text{Fe}/\text{H}] = 0$  dex and  $\xi = 0.66 \text{ km s}^{-1}$ . These values are similar to those recommended by Heiter et al. (2015) as  $(T_{\text{eff}}, \log g) = (5771, 4.438)$ . Element abundances for the Sun were calculated with these model parameters. For HD 218209, the model parameters were obtained from ELODIE and POLARBASE spectrum of the star.

During the calculation of the model atmosphere, the effect of convection on the reported abundances is also taken into consideration. In one-dimensional (1D) atmosphere modeling, it is currently common practice to assume a universal value of 1.5 for the mixing length parameter,  $\alpha$ . However, in order to test the impact of convection on final abundances in this study, the ATLAS models were produced using two different methods for calculating  $\alpha$ . Two well known references in the literature, Ludwig et al. (1999) and Magic et al. (2015), for the calculation of  $\alpha$ , yields two different values (1.59 and 1.98) even when the same set of model parameters is employed. The logarithmic abundance of ionized iron showed a 0.01 dex increase for the model atmosphere computed with the  $\alpha$  parameter set to 1.59 and the model parameters from the ELODIE spectrum. For  $\alpha = 1.98$ , it is +0.02 dex. With regards to the FGK dwarf field stars, it is expected that the influence of the mixing length parameter, for instance, on the determination of metallicity would be minimal, amounting to less than 0.02 dex over eight dwarf stars (Song et al. 2020). Thus, our results for HD 218209 confirm those of Song et al. (2020). Regarding the model parameters of HD 218209 from the POLARBASE spectrum, the logarithmic abundance of ionized iron remained the same for the model atmosphere computed with  $\alpha = 1.59$ . The difference in logarithmic abundance is 0.02 dex for  $\alpha = 1.98$ .

The resulting stellar model parameters for HD 218209 along with our determination of model parameters of the Sun are listed in Table 4. Table 5 lists the model parameters reported for the star in the literature. Rebolo et al. (1988), Abia et al. (1988), and Kim et al. (2016) show the largest variations compared to our  $\log g$ . The abundances obtained for the Solar photosphere as a result of the Solar analysis are given in Table 3. The Solar abundances from Asplund et al. (2009) are also included for comparison. In Table 3, we provide a summary of element abundances based on LTE-based model parameters.  $\log \epsilon$  is the logarithm of the abundances. The errors reported in  $\log \epsilon$  abundances are the  $1\sigma$  line-to-line scatter in abundances.  $[\text{X}/\text{H}]$  is the logarithmic abundance ratio of hydrogen to the corresponding Solar value, and  $[\text{X}/\text{Fe}]$  is the logarithmic abundance considering the Fe I abundance. The error in  $[\text{X}/\text{Fe}]$  is the square root of the sum of the quadratures of the errors in  $[\text{X}/\text{H}]$  and  $[\text{Fe}/\text{H}]$ . Table 3 also presents the abundances obtained using the PolarBase spectrum of the star as  $[\text{X}/\text{Fe}]$  ratio.

#### 4. SUMMARY AND CONCLUSION

We present a line list that can be useful for abundance analysis of G-type stars over 4080 – 6780 Å wavelength region (i.e. for spectra from the ELODIE/SOPHIE library). The line list is expected to be useful for the surveys/libraries with overlapping spectral regions (e.g. ELODIE library, UVES-580 setting of *Gaia*-ESO, and, especially, for the analysis of F- and G-type stars in general. We identified 363 lines of 24 species

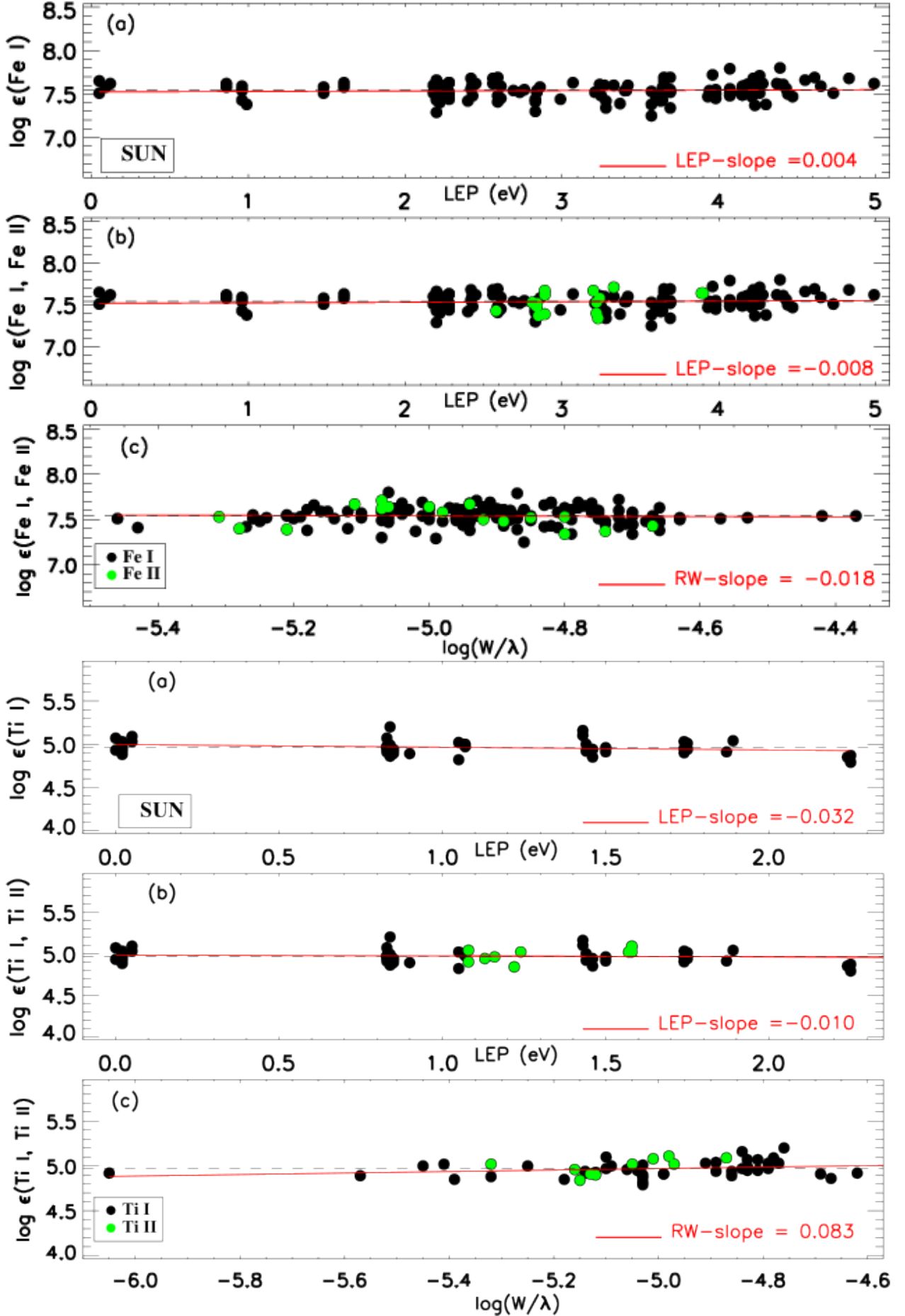


**Figure 3.** An example for the determination of the atmospheric parameters  $T_{\text{eff}}$  and  $\xi$  using abundance ( $\log \epsilon$ ) as a function of both lower LEP (panels a and b for Fe and Ti, respectively) and reduced EW (REW;  $\log (EW/\lambda)$ , panels c for Fe and Ti, respectively) for the Sun. In all panels, the solid red line represents the least-squares fit to the data.

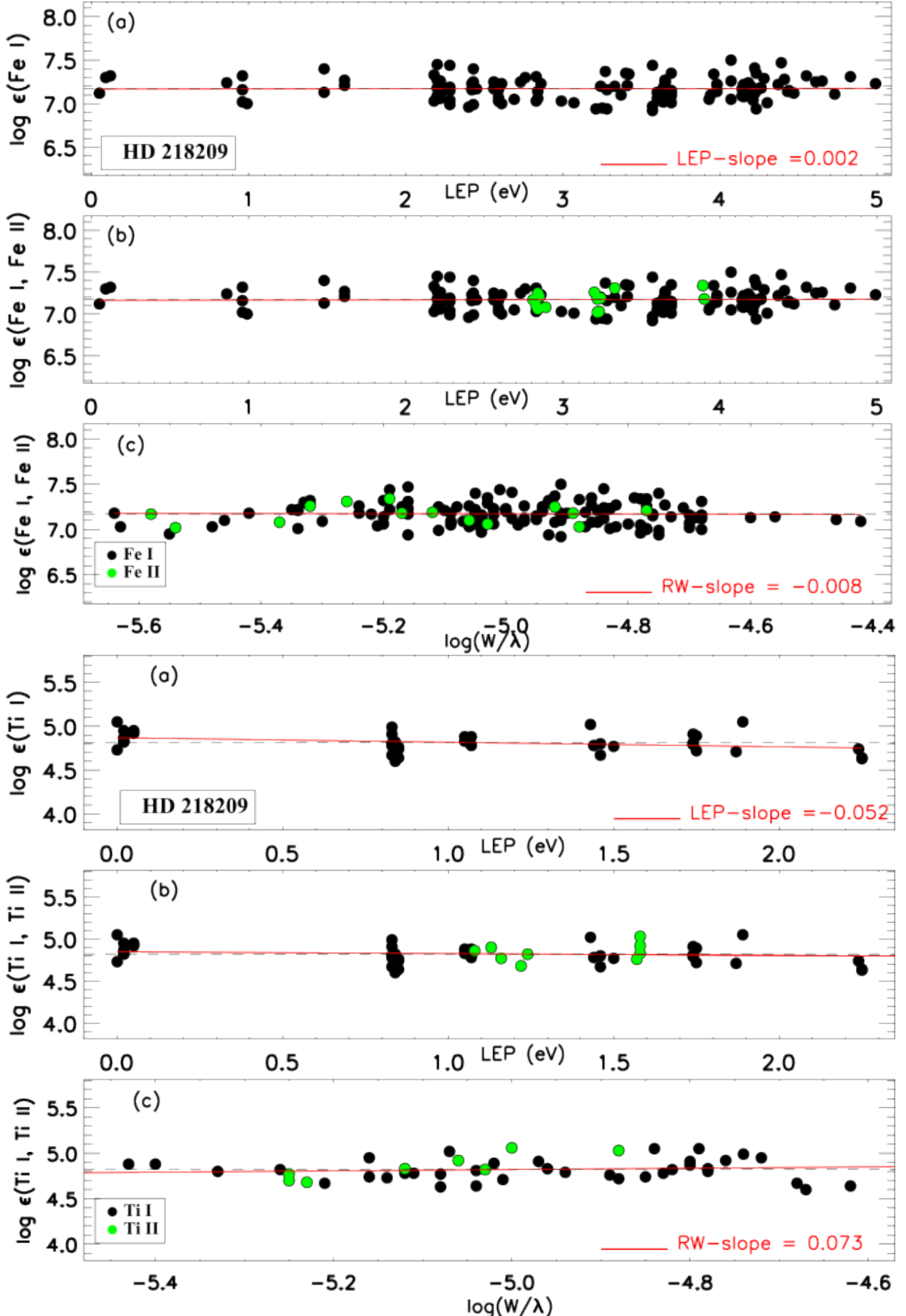


**Figure 4.** An example for the determination of the atmospheric parameters  $T_{\text{eff}}$  and  $\xi$  using abundance ( $\log \epsilon$ ) as a function of both lower LEP (panels a and b for Fe and Ti, respectively) and reduced EW (REW;  $\log(EW/\lambda)$ , panels c for Fe and Ti, respectively) for HD 218209 and the ELODIE spectrum. In all panels, the solid red line represents the least-squares fit to the data.

**Table 5.** Atmospheric parameters of HD 218209 from this study.

$T_{\text{eff}}$ (K)	$\log g$ (cgs)	[Fe/H] (dex)	Notes
5650	4.55	-0.37	This study (ELODIE)
5630	4.43	-0.32	This study (POLARBASE)
5506	4.38	-0.46	<a href="#">Takeda (2023)</a>
5636	4.56	-0.47	<a href="#">Rice &amp; Brewer (2020)</a>
5518	4.39	-0.49	<a href="#">Aguilera-Gómez et al. (2018)</a>
5623	4.46	-0.40	<a href="#">Luck (2017)</a>
5555	4.26	-0.49	<a href="#">Boeche &amp; Grebel (2016)</a>
5565	4.29	-0.49	<a href="#">Boeche &amp; Grebel (2016)</a>
5669	4.24	-0.39	<a href="#">Kim et al. (2016)</a>
5575	4.11	-0.46	<a href="#">Kim et al. (2016)</a>
5607	4.07	-0.58	<a href="#">Kim et al. (2016)</a>
5536	4.37	-0.46	<a href="#">Da Silva et al. (2015)</a>
5705	4.50	-0.43	<a href="#">Mishenina et al. (2015)</a>
5705	4.50	-0.43	<a href="#">Mishenina et al. (2013)</a>
5592	4.25	-0.51	<a href="#">Lee et al. (2011)</a>
5592	4.33	-0.61	<a href="#">Lee et al. (2011)</a>
5592	4.31	-0.65	<a href="#">Lee et al. (2011)</a>
5705	4.50	-0.43	<a href="#">Mishenina et al. (2011)</a>
5539	4.37	-0.50	<a href="#">Da Silva et al. (2011)</a>
5600	–	–	<a href="#">Casagrande et al. (2011)</a>
5473	4.57	-0.64	<a href="#">Sozzetti et al. (2009)</a>
5506	4.38	-0.46	<a href="#">Takeda et al. (2007)</a>
5693	–	–	<a href="#">Masana et al. (2006)</a>
5585	4.60	-0.46	<a href="#">Valenti &amp; Fischer (2005)</a>
5684	–	–	<a href="#">Kovtyukh et al. (2004)</a>
5705	4.50	-0.43	<a href="#">Mishenina et al. (2004)</a>
5665	4.40	-0.60	<a href="#">Gehren et al. (2004)</a>
5478	4.00	-0.60	<a href="#">Rebolo et al. (1988)</a>
5478	4.00	-0.60	<a href="#">Abia et al. (1988)</a>

that have accurate  $gf$ -values and are free of blends in the spectra of the Sun and a Solar analogue star, HD 218209. It should be noted that the GES line list does not contain any atomic transitions below 4200 Å and unlike the GES line list, the line list created in this study contains additional four Fe I, one Fe II, 1 Sc I, 2 Ti I and 1 Co I line below this limit. To assess the uncertainty in  $\log gf$ -values and to minimise systematic errors, we calculated Solar abundances using stellar lines and the high-resolution KPNO spectrum of the Sun. For the creation of the line list in this study, high resolution and high signal to noise ELODIE spectrum of HD 218209 was used. During the comparison with the GES line list, discrepancies in the  $\log gf$  values of some ions were detected. For example, the average difference in  $\log gf$  values for 5 V I lines was  $0.325 \pm 0.328$ . Similarly, for 11 Mn I lines, the difference was  $0.288 \pm 0.283$  dex. The largest difference detected was  $0.585 \pm 0.161$  dex over 6 Co I lines. For the other elements reported in the new line list presented in this study, the  $\log gf$  difference was less than 0.1 dex.

To verify the accuracy of the model parameters obtained for HD 218209 from the ELODIE spectrum, we analyzed the POLARBASE spectrum of the same star. The model parameters from both spectra matched quite well, taking into account the error margins. The element abundances obtained from both spectra also matched quite well, except for Sc I which was represented by a single line at 4023.69 Å in both spectra. The logarithmic abundance from this line in the ELODIE showed a 0.3 dex increase. Additionally, three other species (Sr I, Zr II, and Ce II), with the latter two species presented by two transitions in the spectra, had discrepancies in their logarithmic abundances at around 0.2 dex level. Although the POLARBASE spectrum had higher resolution than the ELODIE, several lines in the POLARBASE did not have clear line profiles. Unfortunately, there was only one spectrum available in the POLARBASE archive, so a more thorough analysis is recommended to check the abundances of the star from the POLARBASE spectrum.

The model parameters obtained for HD 218209 clearly indicate a Solar analogue character for the star. Although no definite classification scheme exists, Solar analogue stars are defined as the dwarf stars of early G-type which have properties analogous to the Sun (e.g. differences in  $T_{\text{eff}}$  and  $\log g$  are  $\pm \leq 100\text{--}200$  K and  $\pm \leq 0.1\text{--}0.2$  dex). Indeed, seeing the star listed in a recent study by Takeda (2023) as a Solar analogue was not surprising for us. The model parameters ( $T_{\text{eff}} = 5506$  K,  $\log g = 4.38$  cgs,  $[\text{Fe}/\text{H}] = -0.46$  dex,  $\xi = 0.74$  km s $^{-1}$ ) reported by Takeda (2023) are in good agreement with those obtained in this study. However, we report up-to-date abundances for the star using 24 species identified in both ELODIE and POLARBASE spectra of the star.

HD 218209 is listed in *Gaia* DR2 (Gaia Collaboration et al. 2018) with *Gaia* DR2 2213415145505277824 designation and a  $T_{\text{eff}}$  of 5648 K. The surface gravity and metallicity of the star were not reported. HD 218209 is also listed in the *Gaia* DR3 (Gaia Collaboration et al. 2023). Our spectroscopic measurements of the temperature and surface gravity of the star align very well with the values reported by the *Gaia* consortium, which are  $T_{\text{eff}} = 5528$  K and  $\log g = 4.40$  cgs. However, there seems to be an error in the reported metallicity of the star by *Gaia*, which states  $[\text{Fe}/\text{H}] = -0.79$  dex. This discrepancy is likely due to the incorrect selection of the template spectrum for the star in the *Gaia* DR3, where the metallicity of the template star is reported as -0.50 dex.

In the *Gaia* DR3 (Gaia Collaboration et al. 2023), an important addition is a collection of 220 million low-resolution BP/RP spectra. The GSP-Phot catalogue provides consistent estimations of stellar parameters for 471 million sources with  $G < 19$  mag, derived from the BP/RP spectra, parallax, and integrated

photometry. It assumes that each source is a single star and that any intrinsic time variability is lost when using combined BP/RP spectra. However, it is important to note that the GSP-Phot results from the BP/RP spectra in the *Gaia* DR3 may still be affected by systematic effects, particularly in the [M/H] estimates with large systematic errors. Consequently, it is advised not to rely on these estimates as they can only provide qualitative information at best ([Beck et al. 2023](#)).

In a study of stellar and sub-stellar companions of nearby stars from the *Gaia* DR2 ([Gaia Collaboration et al. 2018](#)), [Kervella et al. \(2019\)](#) examined the status of stars exhibiting anomalies in their proper motions as binary stars. HD 218209 as a high proper-motion star happens to be one of the common stars. The study found no evidence of a companion around HD 218209, even at distances ranging from 1 to 50 astronomical units (au) and down to planetary masses. Therefore, the authors concluded that HD 218209 is a single star (P. Kervella, private communication, 2023).

[Soubiran & Girard \(2005\)](#), in their exploration of abundance discrepancies between the thin disc and thick disc of the Galaxy, identified HD 218209 out of the 44 stars as being part of the Hercules stream with a likelihood of 0.76. The Hercules stream shares chemical characteristics with the thin disc, which bolsters the dynamic hypothesis (i.e. the influence of the central bar of the Galaxy impacting stars) of its origin. However, kinematic and orbital dynamics analysis for the star is the subject of another study.

## ACKNOWLEDGEMENTS

This study has partly been supported by the Scientific and Technological Research Council (TÜBİTAK) MFAG-121F265. We thank Ferhat Güney for his help with the preparation of Figure 2. We also thank Gizay YOLALAN and Sena A. ŞENTÜRK for helpful discussion.

## REFERENCES

- Abia C., Rebolo R., Beckman J. E., Crivellari L., 1988, *A&A*, **206**, 100
- Aguilera-Gómez C., Ramírez I., Chanamé J., 2018, *A&A*, **614**, A55
- Allende Prieto C., et al., 2008, *Astronomische Nachrichten*, **329**, 1018
- Asplund M., Grevesse N., Sauval A. J., Scott P., 2009, *ARA&A*, **47**, 481
- Bard A., Kock M., 1994, *A&A*, **282**, 1014
- Beck P. G., et al., 2023, *arXiv e-prints*, p. arXiv:2307.10812
- Biemont E., Godefroid M., 1980, *A&A*, **84**, 361
- Biemont E., Grevesse N., Hannaford P., Lowe R. M., 1981, *ApJ*, **248**, 867
- Boeche C., Grebel E. K., 2016, *A&A*, **587**, A2
- Casagrande L., Schönrich R., Asplund M., Cassisi S., Ramírez I., Meléndez J., Bensby T., Feltzing S., 2011, *A&A*, **530**, A138
- Castelli F., Kurucz R. L., 2003, in Piskunov N., Weiss W. W., Gray D. F., eds, Published on behalf of the IAU by the Astronomical Society of the Pacific Vol. 210, Modelling of Stellar Atmospheres. p. A20 ([arXiv:astro-ph/0405087](#)), doi:10.48550/arXiv.astro-ph/0405087
- Da Silva R., Milone A. C., Reddy B. E., 2011, *A&A*, **526**, A71
- Da Silva R., Milone A. d. C., Rocha-Pinto H. J., 2015, *A&A*, **580**, A24
- De Silva G. M., et al., 2015, *MNRAS*, **449**, 2604
- Den Hartog E. A., Lawler J. E., Sneden C., Cowan J. J., 2003, *ApJS*, **148**, 543
- Den Hartog E. A., Lawler J. E., Sobeck J. S., Sneden C., Cowan J. J., 2011, *ApJS*, **194**, 35

- Den Hartog E. A., Lawler J. E., Sneden C., Cowan J. J., Roederer I. U., Sobeck J., 2021, [ApJS](#), **255**, 27
- Fuhr J. R., Wiese W. L., 2006, [Journal of Physical and Chemical Reference Data](#), **35**, 1669
- Gaia Collaboration et al., 2018, [A&A](#), **616**, A11
- Gaia Collaboration et al., 2023, [A&A](#), **674**, A1
- Gehren T., Liang Y. C., Shi J. R., Zhang H. W., Zhao G., 2004, [A&A](#), **413**, 1045
- Gilmore G., et al., 2012, [The Messenger](#), **147**, 25
- Hannaford P., Lowe R. M., Grevesse N., Biemont E., Whaling W., 1982, [ApJ](#), **261**, 736
- Hansen C. J., Bergemann M., Cescutti G., François P., Arcones A., Karakas A. I., Lind K., Chiappini C., 2013, [A&A](#), **551**, A57
- Heijmans J., et al., 2012, in McLean I. S., Ramsay S. K., Takami H., eds, Society of Photo-Optical Instrumentation Engineers (SPIE) Conference Series Vol. 8446, Ground-based and Airborne Instrumentation for Astronomy IV. p. 84460W, doi:10.1117/12.925806
- Heiter U., Jofré P., Gustafsson B., Korn A. J., Soubiran C., Thévenin F., 2015, [A&A](#), **582**, A49
- Heiter U., et al., 2021, [A&A](#), **645**, A106
- Kervella P., Arenou F., Mignard F., Thévenin F., 2019, [A&A](#), **623**, A72
- Kim B., An D., Stauffer J. R., Lee Y. S., Terndrup D. M., Johnson J. A., 2016, [ApJS](#), **222**, 19
- Klose J. Z., Fuhr J. R., Wiese W. L., 2002, [Journal of Physical and Chemical Reference Data](#), **31**, 217
- Kovtyukh V. V., Soubiran C., Belik S. I., 2004, [A&A](#), **427**, 933
- Kurucz R. L., Furenlid I., Brault J., Testerman L., 1984, Solar flux atlas from 296 to 1300 nm
- Lawler J. E., Den Hartog E. A., Sneden C., Cowan J. J., 2006, [ApJS](#), **162**, 227
- Lawler J. E., Sneden C., Cowan J. J., Ivans I. I., Den Hartog E. A., 2009, [ApJS](#), **182**, 51
- Lawler J. E., Guzman A., Wood M. P., Sneden C., Cowan J. J., 2013, [ApJS](#), **205**, 11
- Lawler J. E., Wood M. P., Den Hartog E. A., Feigenson T., Sneden C., Cowan J. J., 2014, [ApJS](#), **215**, 20
- Lawler J. E., Sneden C., Cowan J. J., 2015, [ApJS](#), **220**, 13
- Lawler J. E., Sneden C., Nave G., Den Hartog E. A., Emrahoglu N., Cowan J. J., 2017, [ApJS](#), **228**, 10
- Lawler J. E., Hala Sneden C., Nave G., Wood M. P., Cowan J. J., 2019, [ApJS](#), **241**, 21
- Lee Y. S., et al., 2011, [AJ](#), **141**, 90
- Luck R. E., 2017, [AJ](#), **153**, 21
- Ludwig H.-G., Freytag B., Steffen M., 1999, [A&A](#), **346**, 111
- Magic Z., Weiss A., Asplund M., 2015, [A&A](#), **573**, A89
- Martell S. L., et al., 2017, [MNRAS](#), **465**, 3203
- Masana E., Jordi C., Ribas I., 2006, [A&A](#), **450**, 735
- Meléndez J., Barbuy B., 2009, [A&A](#), **497**, 611
- Mishenina T. V., Soubiran C., Kovtyukh V. V., Korotin S. A., 2004, [A&A](#), **418**, 551
- Mishenina T. V., Gorbaneva T. I., Basak N. Y., Soubiran C., Kovtyukh V. V., 2011, [Astronomy Reports](#), **55**, 689
- Mishenina T. V., Pignatari M., Korotin S. A., Soubiran C., Charbonnel C., Thielemann F. K., Gorbaneva T. I., Basak N. Y., 2013, [A&A](#), **552**, A128
- Mishenina T., Gorbaneva T., Pignatari M., Thielemann F. K., Korotin S. A., 2015, [MNRAS](#), **454**, 1585
- Molaro P., Monai S., 2012, [A&A](#), **544**, A125
- Moore C. E., Minnaert M. G. J., Houtgast J., 1966, The solar spectrum 2935 Å to 8770 Å
- Page B. E. J., Patchett B. E., 1975, [MNRAS](#), **172**, 13
- Pehlivan Rhodin A., Hartman H., Nilsson H., Jönsson P., 2017, [A&A](#), **598**, A102
- Petit P., Louge T., Théado S., Paletou F., Manset N., Morin J., Marsden S. C., Jeffers S. V., 2014, [PASP](#), **126**, 469
- Placco V. M., et al., 2021, [ApJ](#), **912**, L32
- Rebolo R., Molaro P., Beckman J. E., 1988, [A&A](#), **192**, 192

# An Up to Date Line List for Spectroscopic Analysis of F and G Stars

- Rice M., Brewer J. M., 2020, [ApJ, 898, 119](#)
- Shi J. R., Gehren T., Zhao G., 2011, [A&A, 534, A103](#)
- Sneden C. A., 1973, PhD thesis, University of Texas, Austin
- Song N., Alexeeva S., Sitnova T., Wang L., Grupp F., Zhao G., 2020, [A&A, 635, A176](#)
- Soubiran C., Girard P., 2005, [A&A, 438, 139](#)
- Soubiran C., Bienaymé O., Siebert A., 2003, [A&A, 398, 141](#)
- Sozzetti A., Torres G., Latham D. W., Stefanik R. P., Korzennik S. G., Boss A. P., Carney B. W., Laird J. B., 2009, [ApJ, 697, 544](#)
- Steinmetz M., et al., 2006, [AJ, 132, 1645](#)
- Takeda Y., 2023, [Acta Astron., 73, 35](#)
- Takeda Y., Zhao G., Takada-Hidai M., Chen Y.-Q., Saito Y.-J., Zhang H.-W., 2003, [Chinese J. Astron. Astrophys., 3, 316](#)
- Takeda Y., Kawanomoto S., Honda S., Ando H., Sakurai T., 2007, [A&A, 468, 663](#)
- Valenti J. A., Fischer D. A., 2005, [ApJS, 159, 141](#)
- Yanny B., et al., 2009, [AJ, 137, 4377](#)
- Zhao G., Zhao Y.-H., Chu Y.-Q., Jing Y.-P., Deng L.-C., 2012, [Research in Astronomy and Astrophysics, 12, 723](#)
- Şahin T., 2017, [Turkish Journal of Physics, 41, 367](#)
- Şahin T., Bilir S., 2020, [ApJ, 899, 41](#)
- Şahin T., Lambert D. L., 2009, [MNRAS, 398, 1730](#)
- Şahin T., Lambert D. L., Klochkova V. G., Tavolganskaya N. S., 2011, [MNRAS, 410, 612](#)
- Şahin T., Lambert D. L., Klochkova V. G., Panchuk V. E., 2016, [MNRAS, 461, 4071](#)

This paper has been typeset from a  $\text{\TeX}$  /  $\text{\LaTeX}$  file prepared by the author.